JOURNAL OF MATERIALS SCIENCE 31 (1996) 4741–4744

Phase transformation of calcia–alumina–magnesia fibres produced by inviscid melt spinning

YUN-MO SUNG*†, S. A. DUNN‡
†Departments of Materials Science and Engineering and ‡Chemical Engineering, University of Wisconsin-Madison, Madison, WI 53706, USA

$CaO–Al_2O_3–MgO$ (CAM) ceramic fibre produced via inviscid melt spinning (IMS) was investigated for phase transformation. Differential thermal analysis (DTA) on the as-spun CAM fibre gave two transformation peaks, one for exothermic peak at around 927 °C and the other for endothermic one at around 1100 °C. In order to identify each phase transformation x-ray diffraction (XRD) analysis was performed on the CAM fibres heat-treated to each phase transformation completion temperature. The exothermic peak was determined to represent crystallization of remaining amorphous phase in the as-spun CAM fibre. The endothermic peak was determined to correspond to transformation of non-equilibrium $CaO \cdot Al_2O_3$ phase to equilibrium $3CaO \cdot 5Al_2O_3$ phase.

1. Introduction

Development of a high-performance ceramic fibre is one of the key issues in developing high-temperature ceramic matrix composites. Current ceramic fibres produced by chemical vapour deposition, pyrolysis, sol–gel, and slurry processing, are costly due to slow speed of the processes. Furthermore, these fibres contain some porosity and organic remaining, which are related with their production processes.

Inviscid melt spinning (IMS) has been applied to the development of new ceramic fibres. IMS is a much faster and low-cost fibre processing method, compared with the current fibre fabrication techniques. By introducing a reactive hydrocarbon gas such as propane to the ceramic molten stream, Rayleigh break-up, the critical problem in spinning low viscosity ceramic melts, was overcome. A carbon sheath can be formed at the surface of the ceramic molten stream by pyrolysis of the propane gas and this can prevent Rayleigh break-up until solidification occurs. Ceramic fibres of almost theoretical density can be produced in very short time. So far, the ceramic fibres of $CaO–Al_2O_3$(CA) [1–9], $CaO–Al_2O_3–MgO$ (CAM) [10], $BaO–TiO_2$ (BT) [11], $Al_2O_3–ZrO_2$ (AZ) [12], and $Al_2O_3 - MgO$ (AM) [13] were produced by using IMS.

Attempts have been made to spin the CAM fibres using IMS to improve mechanical properties of the CA fibre. Sung and co-workers [10] identified equilibrium phases of $MgO \cdot Al_2O_3$ and α-Al_2O_3, and a non-equilibrium phase of $CaO \cdot Al_2O_3$ in the as-spun CAM fibre. They heat-treated the IMS CAM fibre at 1000 °C for 24 h and found formation of all equilibrium phases of $3CaO \cdot 5Al_2O_3$, $MgO \cdot Al_2O_3$, and α-Al_2O_3. The focus of the present study is on the investigation of the detailed phase transformation of IMS CAM fibre by using differential thermal analysis (DTA) and X-ray diffraction (XRD).

2. Experimental procedure

The unique IMS apparatus mainly consists of three parts: (1) an induction heating unit, (2) a graphite crucible with orifice at the bottom and associated gas plate assembly, and (3) two containment chambers (furnace and intermediate chambers). Special care was taken for heat insulation to obtain high temperature. Fig. 1 shows an overall schematic diagram of the IMS unit [14].

High purity $CaCO_3$, Al_2O_3, and MgO powders were well mixed using zirconia ball-milling. The mixed powders ($\sim$ 100 g) were loaded inside the graphite crucible and heated in a vacuum atmosphere (6.68 Pa) by induction heating (maximum capacity of 15 kW and 10 kHz). Before melting the powders at 1680 °C, both the furnace and intermediate chambers were filled with nitrogen gas at a pressure of $\sim 3.44 \times 10^5$ Pa to prevent violent gas evolution from the melt. To homogenize the melt, temperature was held at 1700 °C for 20 min. When the slide valve between intermediate and catch chamber was opened, the intermediate chamber quickly dropped to an atmospheric pressure. The pressure difference between the furnace chamber and the intermediate chamber

*Present address of author to whom all correspondence should be addressed: Department of Materials and Engineering, Daejin University, Pochun-kun, Kyungki-do 487-800, Korea.

0022–2461

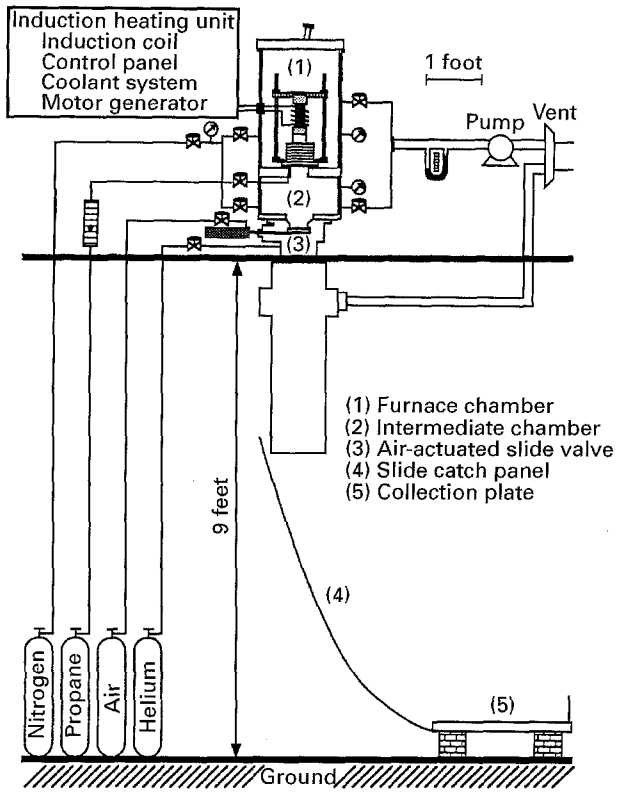

Figure 1 Schematic diagram of the overall inviscid melt-spinning (IMS) apparatus [14].

extruded the molten CAM through the orifice and into the intermediate chamber atmosphere. Once the molten stream was continuously flowing as droplets, the reactive gas (propane) was introduced through the gas plates. The carbon deposition on the molten stream results from pyrolysis of propane gas by the heat from the molten stream as follows

$$C_3H_8(g) \xrightarrow{\text{heat}} 3C(s) + 4H_2(g) \quad (1)$$

The microstructure of the as-spun CAM fibre was examined using scanning electron microscopy (SEM; Jeol SEM 35-C). Differential thermal analysis (Perkin-Elmer DTA 1700) was performed to investigate the phase transformation of this fibre. The CAM fibres ($\sim$ 1 cm long and total weight of 100 mg) were loaded inside a platinum crucible and heated from 25 to 1400 °C at a heating rate of 10 °C min^{-1} in an air atmosphere. DTA temperatures were calibrated using pure Al and Cu. To identify crystalline phases in the as-spun CAM fibres, powdered CAM fibres were investigated using an XRD (Nicolet Stóe Transmission/Bragg-Brentano) with a Cu-Kα source, 15 s time constant, 5 to 90° scan range, and 0.02 ° step size. The as-spun CAM fibres were heated from room temperature to 955 and 1180 °C, respectively at a heating rate of 10 ° min^{-1} inside a horizontal furnace in an air atmosphere. The heat-treated CAM fibres were ground and phase analysed by using XRD. The resulting XRD patterns were identified using the Joint Committee on Powder Diffraction Standards (JCPDS) cards [15].

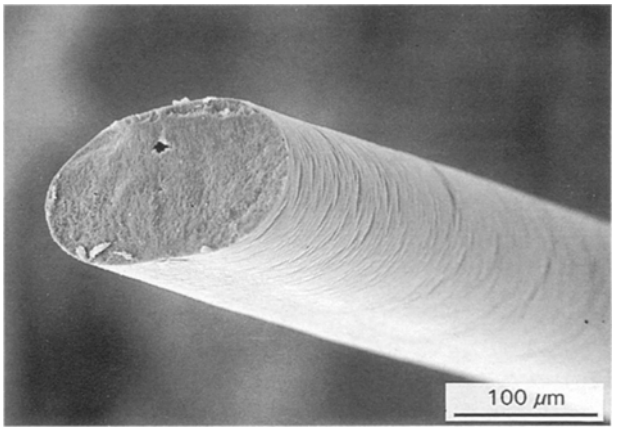

Figure 2 Scanning electron micrograph of IMS $CaO–Al_2O_3–MgO$ fibre [10].

3. Results and discussion

The IMS CAM fibres were approximately 180 μm in diameter and 10 cm in length as produced via IMS. The fibres were slightly curly and the faces were elliptical in shape. The elliptical face would be related with the shape of an orifice which was made by mechanical drilling. The surface of the fibres was slightly rough, indicating that these fibres are crystalline. Most of the IMS CAM fibres showed small porosity which might be related with possible gas evolution during cooling or shrinkage during solidification. Fig. 2 shows a SEM of the IMS CAM fibre.

Thermodynamic stability of a mixture of molten CaO, Al_2O_3, and MgO against reduction by carbon at 1700 °C was examined as follows [16]

$$CaO + C \rightarrow Ca + CO$$

$$\Delta G^\circ = +125.9\,kJ\,mol^{-1} \quad \text{at } 1700\,^\circ C \quad (2)$$

$$Al_2O_3 + 3C \rightarrow 2Al + 3CO$$

$$\Delta G^\circ = +190.7\,kJ\,mol^{-1} \quad \text{at } 1700\,^\circ C \quad (3)$$

$$MgO + C \rightarrow Mg + CO$$

$$\Delta G^\circ = +675.6\,kJ\,mol^{-1} \quad \text{at } 1700\,^\circ C \quad (4)$$

These positive values of the free energy of formation imply that all of the three oxides would be stable against reduction by carbon at 1700 °C.

DTA was performed to examine a possible phase transformation in the IMS CAM fibre. Fig. 3 presents the DTA curve of the IMS CAM fibre. One exothermic peak ranging from 872 to 955 °C and one endothermic peak ranging from 1033 to 1180 °C are shown. The peak temperature values were 927 and 1100 °C, respectively.

In order to identify each phase transformation the CAM fibres were heated from room temperature to 955 and 1180 °C, respectively, at a heating rate of 10 °C min^{-1} inside a furnace. The as-spun CAM fibres and heat-treated CAM fibres were ground and analysed by using XRD. Fig. 4 shows the XRD patterns from the as-spun CAM fibres (a), the CAM fibres heated to 955 °C (b), and the CAM fibres heated to 1180 °C (c). The XRD patterns of the as-spun CAM

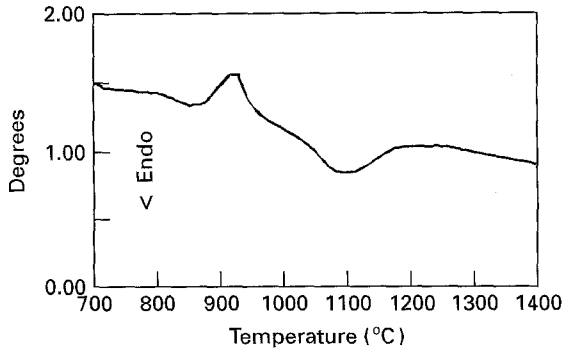

Figure 3 Differential thermal analysis curve of as-spun $CaO–Al_2O_3–MgO$ fibre at a heating rate of 10 °C min^{-1} in the air atmosphere. Both exothermic and endothermic peaks are shown.

fibres showed many peaks from the crystalline phases, and a big hump and smooth hill ranging from 5 to 40°, which certainly represents the existence of an amorphous phase. By comparing the positions and intensities of the peaks with the data in the JCPDS cards, $MgO \cdot Al_2O_3$, $CaO \cdot Al_2O_3$, and α-Al_2O_3 phases were identified. The peak positions of the $MgO \cdot Al_2O_3$ phase are shifted approximately -0.002 nm, compared with the data in the JCPDS card. This would result from formation of $MgO \cdot Al_2O_3$ solid solution rather than formation of stoichiometric $MgO \cdot Al_2O_3$.

Fig. 5 shows a phase diagram of the $CaO–Al_2O_3–MgO$ system [17]. Table I shows the phase compositions shown in Fig. 5. Point 6 corresponds to the composition of the CAM fibre produced for the present study. The phase diagram shows that at this composition the equilibrium phases are $3CaO \cdot 5Al_2O_3$, $MgO \cdot Al_2O_3$, and α-Al_2O_3. Therefore, the $CaO \cdot Al_2O_3$ phase in the as-spun CAM fibre is a non-equilibrium phase.

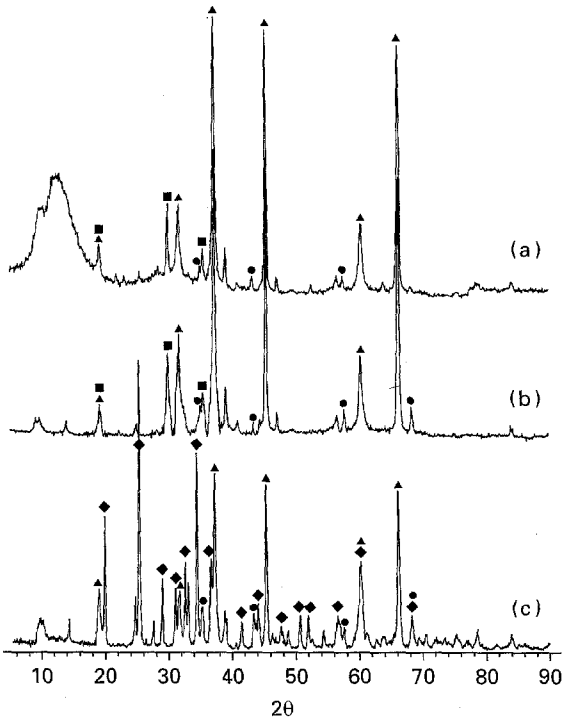

Figure 4 X-ray diffraction patterns of (a) as-spun $CaO–Al_2O_3–MgO$ (CAM) fibre, (b) CAM fibre heat-treated to 955 °C, and (c) CAM fibre heat-treated to 1180 °C. The as-spun CAM fibre shows formation of equilibrium phases of $MgO \cdot Al_2O_3$ (▲) and α-Al_2O_3 (●), and a non-equilibrium phase of $CaO \cdot Al_2O_3$ (■) as well as non-crystallinity. In the CAM fibre heat-treated to 955 °C non-crystallinity has disappeared. The CAM fibre heat-treated to 1180 °C showed formation of all the equilibrium phases of $3CaO \cdot 5Al_2O_3$ (◆), $MgO \cdot Al_2O_3$ (▲), and α-Al_2O_3 (●).

In the XRD patterns of the CAM fibres heat-treated to 955 °C, the hump and hill shown in Fig. 4(a) had disappeared. This implies that the amorphous phase in the as-spun CAM fibre was crystallized during the

TABLE I Phase compositions of the $CaO–Al_2O_3–MgO$ system shown in Fig. 5

Points	Crystal phases	Composition (wt%)			Temperature (°C)
		CaO	MgO	Al_2O_3	
A	C, M	67.0	33.0	–	2300
B	M, MA	–	45.0	55.0	2030
C	MA, A	–	2.0	98.0	1925
D	C, C_3A	59.0	–	41.0	1535
E	C_3A, C_5A_3	50.0	–	50.0	1395
F	C_5A_3, CA	47.0	–	53.0	1400
G	CA, CA_5	33.5	–	66.5	1590
H	CA_5, A	24.0	–	76.0	1700
1	M, C, C_3A	51.5	6.2	42.3	1450
2	M, C_3A, C_5A_3	46.0	6.3	47.7	1345
3	M, C_5A_3, CA	41.5	6.7	51.8	1345
4	M, MA, CA	45.7	6.9	52.4	1370
5	MA, CA, CA_5	21.0	5.0	74.0	1680
	$5CaO \cdot 3Al_2O_3$	47.8	–	52.2	1455
	$CaO \cdot Al_2O_3$	35.4	–	64.6	1600
	$3CaO \cdot 5Al_2O_3$	24.8	–	75.2	1720
	$MgO \cdot Al_2O_3$	–	28.4	71.6	2135
	$3CaO \cdot Al_2O_3$	62.2	–	37.8	1535
	Periclase (M)	–	100.0	–	2800
	Lime (C)	100.0	–	–	2570
	Corundum (A)	–	–	100.0	2050

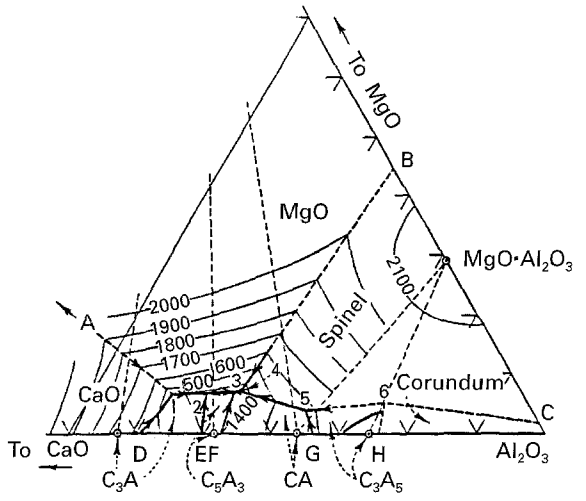

Figure 5 Phase diagram of the $CaO–Al_2O_3–MgO$ system [17].

heat treatment. Therefore, it can be concluded that the exothermic peak in the DTA curve corresponds to the crystallization of the amorphous phase in the as-spun CAM fibres. The peaks in the patterns again came from $CaO \cdot Al_2O_3$, $MgO \cdot Al_2O_3$, and α-Al_2O_3 phases. Any other phase was not identified from the XRD patterns.

Fig. 4(c) shows the XRD patterns of the CAM fibres heat-treated to 1180 °C. A new phase, $3CaO \cdot 5Al_2O_3$, was identified as a major phase and the $MgO \cdot Al_2O_3$ and α-Al_2O_3 phases were also identified. The $CaO \cdot Al_2O_3$, the phase in the as-spun CAM fibre, had disappeared. From this XRD analysis, it can be concluded that the endothermic peak in the DTA curve corresponds to the transformation of the non-equilibrium $CaO \cdot Al_2O_3$ phase to the equilibrium $3CaO \cdot 5Al_2O_3$ phase. All the three phases in this heat-treated fibre were the equilibrium phases, as shown in Fig. 5.

4. Conclusions

The inviscid melt-spun $CaO–Al_2O_3–MgO$ (CAM) fibre showed a small amount of porosity which might be related with gas evolution, or shrinkage during cooling. DTA on the as-spun CAM fibre showed one exothermic peak ranging from 872 to 955 °C and one endothermic peak ranging from 1033 to 1180 °C. The XRD on the as-spun CAM fibre showed some degree of non-crystallinity, as well as formation of equilibrium phases of $MgO \cdot Al_2O_3$ and α-Al_2O_3, and a non-equilibrium phase of $CaO \cdot Al_2O_3$. The XRD patterns of the CAM fibre heat-treated to 955 °C showed peaks from the phases of $MgO \cdot Al_2O_3$, α-Al_2O_3, and $CaO \cdot Al_2O_3$. Non-crystallinity of the fibre had disappeared. The exothermic peak in the DTA curve was determined to present crystallization of the amorphous phase. The XRD patterns of the CAM fibre heat-treated to 1180 °C showed formation of $3CaO \cdot Al_2O_3$ phase as well as $MgO \cdot Al_2O_3$ and α-Al_2O_3 phases. The non-equilibrium phase, $CaO \cdot Al_2O_3$, in the as-spun CAM fibre had disappeared. Therefore, the endothermic peak in the DTA curve was determined to correspond to transformation of the non-equilibrium phase, $CaO \cdot Al_2O_3$ to the equilibrium phase, $3CaO \cdot 5Al_2O_3$.

Acknowledgements

The authors would like to thank Dr Sungtae Kim at the University of Wisconsin-Madison for kindly providing access to DTA.

References

1. R. E. CUNNINGHAM, L. F. RAKESTRAW and S. A. DUNN, in "Spinning wire from molten metal" AIChE Symposium Series, Vol. 74, edited by J. W. Mottern and W. J. Privott (American Institute of Chemical Engineers, NY, 1978) p. 20.
2. B. S. MITCHELL, K. Y. YON, S. A. DUNN and J. A. KOUTSKY, *Mater. Lett.* **10** (1990) 71.
3. F. T. WALLENBERGER, N. E. WESTON and S. A. DUNN, *J. Non-Cryst. Solids* **24** (1990) 116.
4. *Idem., J. Mater. Res.* **5** (1990) 2682.
5. *Idem., SAMPE Quart.* **9** (1990) 121.
6. F. T. WALLENBERGER, *Ceram. Bull.* **69** (1990) 1646.
7. F. T. WALLENBERGER, N. E. WESTON, K. MOTZFELT and D. G. SWARTZFAGER, *J. Amer. Ceram. Soc.* **75** (1992) 629.
8. B. S. MITCHELL, K. Y. YON, S. A. DUNN and J. A. KOUTSKY, *J. Non-Cryst. Solids* **152** (1993) 143.
9. Y.-M. SUNG, S. A. DUNN and J. A. KOUTSKY, *Ceram. Inter.* **21** (1995) 169.
10. *Idem., Ibid* **20** (1994) 337.
11. B. S. MITCHELL, K. Y. YON, S. A. DUNN and J. A. KOUTSKY, *Chem. Engr. Comm.* **106** (1991) 87.
12. Y.-M. SUNG, S. A. DUNN and J. A. KOUTSKY, *J. Mater. Sci.* **30** (1995) 5995.
13. *Idem., ibid*, in press 1996.
14. K.-Y. YON, Ph.D. Thesis, University of Wisconsin-Madison (1993).
15. JANAF Thermochemical Tables, 2nd Edn. National Standard Reference Data System (1971).
16. D. R. GASKELL, 'Introduction to metallurgical thermodynamics," 2nd Edn (McGraw-Hill) (1981).
17. G. A. RANKIN and H. E. MERWIN, *J. Amer. Chem. Soc.* **38** (1916) 568.

Received 1 November 1995
and accepted 13 February 1996